UNIVERSITY OF LEEDS

This is a repository copy of *Characterisation of columnar inertial modes in rapidly rotating spheres and spheroids*.

White Rose Research Online URL for this paper:
http://eprints.whiterose.ac.uk/119474/

Version: Accepted Version

Article:
Maffei, S, Jackson, A and Livermore, PW orcid.org/0000-0001-7591-6716 (2017) Characterisation of columnar inertial modes in rapidly rotating spheres and spheroids. Proceedings of the Royal Society A: Mathematical, Physical and Engineering Sciences, 473 (2204). ISSN 1364-5021

https://doi.org/10.1098/rspa.2017.0181

© 2017, Royal Society of London. This is an author produced version of a paper published in Proceedings of the Royal Society A: Mathematical, Physical and Engineering Sciences. Uploaded in accordance with the publisher's self-archiving policy.

Reuse
Items deposited in White Rose Research Online are protected by copyright, with all rights reserved unless indicated otherwise. They may be downloaded and/or printed for private study, or other acts as permitted by national copyright laws. The publisher or other rights holders may allow further reproduction and re-use of the full text version. This is indicated by the licence information on the White Rose Research Online record for the item.

Takedown
If you consider content in White Rose Research Online to be in breach of UK law, please notify us by emailing eprints@whiterose.ac.uk including the URL of the record and the reason for the withdrawal request.

White Rose university consortium
Universities of Leeds, Sheffield & York

eprints@whiterose.ac.uk
https://eprints.whiterose.ac.uk/

Characterisation of columnar inertial modes in rapidly rotating spheres and spheroids

Stefano Maffei,[1,2] Andrew Jackson,[1] and Philip W. Livermore[3]

[1)] *Institute for Geophysics, ETH Zürich, CH-8092, Switzerland*

[2)] *Department of Physics, University of Colorado, Boulder, Colorado 80309, USA*

[3)] *School of Earth and Environment, University of Leeds, Leeds, LS2 9JT, UK*

(Dated: 24 July 2017)

We consider fluid-filled spheres and spheroidal containers of eccentricity ϵ in rapid rotation, as a proxy for the interior dynamics of stars and planets. The fluid motion is assumed to be quasi-geostrophic (QG): horizontal motions are invariant parallel to the rotation axis z, a characteristic which is handled by use of a stream function formulation which additionally enforces mass conservation and non-penetration at the boundary. By linearising about a quiescent background state, we investigate a variety of methods to study the QG inviscid inertial wave modes which are compared with fully 3-D calculations. We consider the recently-proposed weak formulation of the inviscid system valid in spheroids of arbitrary eccentricity, to which we present novel closed-form polynomial solutions. Our modal solutions accurately represent, in both spatial structure and frequency, the most z-invariant of the inertial wave modes in a spheroid, and constitute a simple basis set for the analysis of rotationally-dominated fluids. We further show that these new solutions are more accurate than those of the classical axial-vorticity equation, which is independent of ϵ and thus fails to properly encode the container geometry. We also consider the effects of viscosity for the cases of both no-slip and stress-free boundary conditions for a spherical container. Calculations performed under the columnar approximation are compared with 3-D solutions and excellent agreement has been found despite fundamental differences in the two formulations.

Keywords: Inertial modes, quasi-geostrophy, Earth's outer core

I. INTRODUCTION

It is well accepted (since Larmor (1919)) that planetary magnetic fields observed on Earth and other planets have their origin in the fluid motions powered by thermo-chemical convection in their outer cores through the geodynamo mechanism (Roberts and Aurnou, 2012). The presence of rotation, thermal and chemical heterogeneities, magnetic forces and viscosity makes the entire system dynamic and complex. In the Earth's core, rotation is thought to be the dominant force acting on the system as illustrated by the smallness of the large scale Rossby (Ro) and Ekman (E) numbers. These numbers are a measure of the importance of inertial and viscous forces with respect to the Coriolis force and they have accepted estimates of $Ro \simeq^{-6}$ and $E \simeq 10^{-15}$ (Olson, 2015); as a consequence the Earth's outer core is said to be in rapid rotation.

One of the main characteristics of rapidly rotating systems is that the dynamics tends to be independent along the vertical direction defined by the axis of rotation. This is a consequence of the Taylor-Proudman theorem (Pedlosky, 1992) which states that large scale, slow motions in the presence of fast rotation are governed at leading order by a balance between the Coriolis force and the pressure gradient (the geostrophic balance). Flows strictly governed by the geostrophic balance are invariant along the vertical direction and therefore bi-dimensional. The tendency of rapidly rotating dynamics to be columnar has been documented in experiments (Cardin and Olson, 1994) and numerical simulations of thermal convection in spherical geometries (Zhang, 1992; Christensen, 2002) and in geodynamo simulations (Kageyama, Miyagoshi, and Sato, 2008). Furthermore, inversion of geomagnetic observations reveals that the core surface flows possess a high degree of equatorial symmetry (Hulot, Le Mouël, and Jault, 1990; Gillet, Schaeffer, and Jault, 2011) in agreement with the presence of columnar flows in the interior.

The other forces that are important in the dynamics are buoyancy and magnetic (Lorentz) forces. Although in principle the presence of buoyancy can weaken the Taylor-Proudman constraint (see the discussion in Jacobs (1987), chapter 4), it has been shown through numerical and experimental studies (Christensen, 2002; Yadav *et al.*, 2016; Cardin and Olson, 1994) that buoyancy does not completely destroy the vertical invariance of the flows, even in strongly forced regimes. Similar considerations are valid for the Lorentz force, as the presence of a strong magnetic field can inhibit the flows in the direction perpendicular to

the field lines. This law, called the Ferraro law (Ferraro, 1937) can clearly be in competition with the vertical invariance imparted by rapid rotation if the magnetic field is strong enough (Davidson, 2013). It has been shown in Jault (2008) and Gillet, Schaeffer, and Jault (2011) that transient motions remain highly columnar as long as the Lehnert number (Le), a measure of the importance of the Lorentz force with respect to rotation, is smaller than 10^{-2} and magnetic diffusivity is negligible. Based on estimated values of magnetic field intensity in the Earth's core (Gillet *et al.*, 2010) it can be concluded that these constraints are valid for motions with interannual to decadal timescales.

Evidence for the presence of columnar motions has paved the way for the development of models, based on the quasi-geostrophic (QG) approximation, in which it is assumed that horizontal flows have a columnar structure (i.e. invariant along the vertical) and the non-penetration condition at the core-mantle boundary (CMB) is satisfied by requiring that the vertical flows have a linear vertical dependence. These kinds of models have first been developed for studies of thermal convection (Cardin and Olson, 1994; Aubert, Gillet, and Cardin, 2003; Gillet and Jones, 2006; Guervilly and Cardin, 2016) and are now being considered for studying the dynamics of the Earth's core in presence of magnetic fields (Schaeffer and Cardin, 2005, 2006; Canet, Fournier, and Jault, 2009; Canet, Finlay, and Fournier, 2014; Labbé, Jault, and Gillet, 2015). The power of these models has recently been illustrated in Guervilly and Cardin (2016), in which thermal convection has been studied for Ekman numbers in the range $10^{-8} \leq E \leq 10^{-5}$ and Prandtl numbers (Pr, the ratio of viscosity over thermal diffusivity) in the range $10^{-2} \leq Pr \leq 10^{-1}$. Decreasing the Ekman number down to $E \leq 10^{-7}$, Guervilly and co-authors where able to observe a transition to a "strong branch" regime (characterised by more vigorous and efficient convection with respect to the better known "weak branch") and sub-critical convection. Studying these same dynamics in 3-D is out of reach of current direct numerical simulations whose cutting edge is at $E \simeq 10^{-6}$ and $Pr \simeq 1$ (King, Stellmach, and Aurnou, 2012) and it is difficult for them to study this phenomenology.

Due to the presence of the Coriolis force, inertial waves can propagate in the outer core (Greenspan, 1968) and eventually normal modes (also called inertial oscillations) can be established. The frequency of these oscillations is constrained to be less that twice the rotation frequency of the fluid and at low frequency the oscillations becomes highly elongated along the vertical direction (Zhang *et al.*, 2001). Calculation of the inertial eigenmodes and

eigenfrequencies under the columnar approximation is useful for characterising the QG models and phenomenology in many ways. Columnar inertial oscillations propagate eastward, in agreement with the propagation of Rossby waves in the atmosphere (Canet, Finlay, and Fournier, 2014). In the presence of a magnetic field, another class of oscillation emerges, travelling westward with longer periods and which might possibly be the cause of the westward drift of geomagnetic features observed at the CMB (Hide, 1966; Jackson, 2003). The magnetic solution can be characterised in terms of the inertial oscillations and in some cases (Malkus, 1967; Schmitt, 2010; Canet, Finlay, and Fournier, 2014) eigenmodes and eigenfrequencies can be explicitly calculated from the inertial ones. At the onset of thermal convection the hydrodynamic instability sets in as a set of perturbed, QG inertial modes (Zhang, 1994, 1995) so that the sole knowledge of columnar inertial modes is sufficient to calculate the onset of thermal convection with excellent agreement with 3-D numerical simulations (Zhang and Liao, 2004; Zhang, Liao, and Busse, 2007; Zhang, Lam, and Kong, 2017). Furthermore it has recently been shown that the 3-D inertial modes in a sphere (Ivers, Jackson, and Winch, 2015) and in ellipsoids (Vantieghem, 2014; Backus and Rieutord, 2017; Ivers, 2017) form a complete polynomial set. The proof of completeness of the columnar inertial modes would pose solid theoretical foundations behind the resolution of generic QG motions on a complete basis set.

The purpose of the present paper is to characterise the inertial modes in a spherical container in rapid rotation by means of the columnar flow approximation. The structure of the paper is the following: Section II is devoted to the introduction of the governing equations and the QG formulation studied throughout the paper. In Section III we study the inviscid problem containing the essence of inertial wave propagation. For the first time to our knowledge, we propose a fully analytical solution for the normal mode problem that rests on the axial vorticity equation formalism, which is commonplace in the development of QG models. A more general formulation, proposed in Labbé, Jault, and Gillet (2015) allows the calculation of QG solutions that are in better agreement with 3-D calculations. In Section IV we analyse this alternative formulation in some detail and we derive an analytical solution for QG inertial modes in oblate spheroid of arbitrary eccentricity. This general solution allows for a unification of the axial vorticity formalism and the approach of Labbé, Jault, and Gillet (2015). A comparison of our QG solution with known 3-D results (Zhang *et al.*, 2001; Zhang, Liao, and Earnshaw, 2004) is presented in Section V. In Section VI we study

the effect of viscosity on the novel QG analytical solution in the case of both no-slip and stress-free conditions at the surface of the domain. A review of the formulation for finding the viscous correction to the inertial mode eigenfrequencies, decay rate and boundary flows is reported and specialised to the QG case. Comparison with 3-D calculations is presented. Discussions and conclusions can be found in Section VII.

II. GOVERNING EQUATIONS

Consider a rotating fluid sphere of radius r_0 whose axis of rotation passing through the center of the sphere we indicate with $\mathbf{\Omega}$. Since we are considering motions that are almost invariant along the vertical direction defined by the rotation axis, we introduce a cylindrical coordinate system with unit vectors $(\mathbf{e}_s, \mathbf{e}_\phi, \mathbf{e}_z)$ whose vertical unit vector is aligned with $\mathbf{\Omega}$:

$$\mathbf{e}_z = \frac{\mathbf{\Omega}}{|\mathbf{\Omega}|}. \tag{1}$$

Then s is the distance from the rotation axis and ϕ the longitude. This reference system is common in studies of columnar flows in the outer core (see for example Cardin and Olson (1994); Aubert, Gillet, and Cardin (2003); Canet, Fournier, and Jault (2009); Canet, Finlay, and Fournier (2014); Labbé, Jault, and Gillet (2015) and Guervilly and Cardin (2016)). We will also make use of a spherical coordinate system $(\mathbf{e}_r, \mathbf{e}_\theta, \mathbf{e}_\phi)$ where r is the distance from the center of the sphere, θ is the colatitude and ϕ the longitude. The relationship between the spherical and cylindrical systems are the following:

$$s = r\sin\theta \tag{2}$$

$$z = r\cos\theta. \tag{3}$$

In cylindrical coordinates the boundary $r = r_0$ is also defined as $z = \pm\sqrt{r_0^2 - s^2}$, with $2\sqrt{r_0^2 - s^2}$ being the height of the sphere at any point defined by a distance s from the rotation axis.

We consider that the fluid is incompressible and that no flow is permitted across the boundary of the spherical container. The momentum equation describing the evolution of the velocity $\mathbf{u}$ is the Navier-Stokes equation:

$$\frac{\partial \mathbf{u}}{\partial t} + (\mathbf{u}\cdot\nabla)\mathbf{u} + 2\mathbf{\Omega}\times\mathbf{u} = -\frac{1}{\rho}\nabla P + \nu\nabla^2\mathbf{u} + \frac{1}{\rho}\mathbf{F} \tag{4}$$

where ρ is the density of the fluid, P is the pressure, ν the kinematic viscosity and $\mathbf{F}$ are the body forces (such as buoyancy) that are neglected in the present study. In analogy to Zhang and Liao (2004), we non-dimensionalise the governing equations by measuring time and distances in terms of $|\mathbf{\Omega}|^{-1}$ and r_0, respectively. Velocity and pressure are then normalised in terms of $|\mathbf{\Omega}|r_0$ and $\rho r_0^2|\mathbf{\Omega}|^2$, respectively and the relevant system then is

$$\frac{\partial \mathbf{u}}{\partial t} + 2\mathbf{e}_z \times \mathbf{u} + \nabla P = 2E\nabla^2 \mathbf{u} \tag{5}$$

$$\nabla \cdot \mathbf{u} = 0 \tag{6}$$

$$\mathbf{e}_r \cdot \mathbf{u}|_{r=1} = 0 \tag{7}$$

$$\mathbf{e}_r \times \mathbf{u}|_{r=1} = 0 \quad \text{(no-slip)} \tag{8}$$

$$\frac{\partial}{\partial r}\left(\frac{u_\theta}{r}\right)\Big|_{r=1} = \frac{\partial}{\partial r}\left(\frac{u_\phi}{r}\right)\Big|_{r=1} = 0 \quad \text{(stress-free)} \tag{9}$$

where the Ekman number E has been defined as:

$$E = \frac{\nu}{2|\mathbf{\Omega}|r_0^2}. \tag{10}$$

Equation (5) is then the non-dimensional form of the momentum equation in absence of body forces, (6) expresses the divergence free condition of the fluid and (7) is the non-penetration boundary condition. Under the inviscid approximation $E = 0$ and (7) is sufficient given the order of the momentum equation. But real fluids have finite viscosity for which $E > 0$ and we must provide an additional boundary condition on the flow. Typical choices are either no-slip (8) or stress-free (9); the first is appropriate for describing a rigid surface like the CMB, while the latter is applicable to the outer surface of gas giants or stars.

As long as rotation dominates over all other forces, the momentum equation (5) is amenable to a perturbative analysis where the leading order is the geostrophic balance. In a closed container whose shape is symmetric around the rotation axis such as a sphere, solutions to the resulting equation are time independent zonal flows invariant along both z and ϕ. These geostrophic flows clearly are not representative of the complex dynamics taking place in fluid planetary cores and subdominant orders have to be considered (Gillet, Schaeffer, and Jault, 2011), hence the quasi-geostrophic approximation. The QG approach considered here is described in Cardin and Olson (1994); Schaeffer and Cardin (2006) and Canet, Finlay, and Fournier (2014) and consists of imposing the velocity field to be of the

form:

$$\mathbf{u}(s,\phi,z) = \frac{1}{H}\nabla\times(\Psi(s,\phi)\mathbf{e}_z) - \frac{sz}{H^2}u_s(s,\phi)\mathbf{e}_z = \frac{1}{sH}\frac{\partial\Psi}{\partial\phi}\mathbf{e}_s - \frac{1}{H}\frac{\partial\Psi}{\partial s}\mathbf{e}_\phi - \frac{z}{H^3}\frac{\partial\Psi}{\partial\phi}\mathbf{e}_z \quad (11)$$

where

$$H = \sqrt{1-s^2}. \quad (12)$$

Together with the boundary condition

$$\Psi(s=1) = 0 \quad (13)$$

this formulation describes a columnar flow that satisfies non-penetration boundary condition over the entire outer boundary (7), the incompressibility constraint (6) and it is entirely defined by the 2-D scalar potential $\Psi(s,\phi)$ that we refer to as a stream function.

III. INERTIAL NORMAL MODES

For now we neglect viscous effects and impose $E = 0$ in (5)

$$\frac{\partial\mathbf{u}}{\partial t} + 2\mathbf{e}_z\times\mathbf{u} + \nabla P = 0. \quad (14)$$

We then consider normal mode solutions of the form

$$\mathbf{u}(s,z,\phi,t) = \hat{\mathbf{u}}(s,z)\mathrm{e}^{\mathrm{i}(m\phi+\omega t)} \quad (15)$$

with $m \geq 1$, and similarly for the pressure P, where m is the azimuthal wavenumber, ω the oscillation frequency of the solution and the hat indicates a function of the meridional coordinates (s,z). Given the definition (11) an equivalent ansatz is:

$$\Psi(s,\phi,t) = \hat{\Psi}(s)\mathrm{e}^{\mathrm{i}(m\phi+\omega t)}. \quad (16)$$

Substituting (15) in the inviscid momentum equation we obtain the following normal mode equation

$$\mathrm{i}\omega\mathbf{u} + \nabla P + 2\mathbf{e}_z\times\mathbf{u} = 0 \quad (17)$$

which is treated in detail in Kudlick (1966) and Greenspan (1968). A well known procedure (see for example Aubert, Gillet, and Cardin (2003); Canet, Finlay, and Fournier (2014) and references therein) to eliminate pressure from the momentum equation is to consider the

axial vorticity equation by taking the curl of (14). The vertical component of the resulting equation is the axial vorticity equation:

$$\left[\frac{\partial}{\partial s}\left(\frac{s}{H}\frac{\partial}{\partial s}\right)+\frac{1}{sH}\frac{\partial^2}{\partial\phi^2}\right]\frac{\partial\Psi}{\partial t}-2\frac{s}{H^3}\frac{\partial\Psi}{\partial\phi}=0. \tag{18}$$

By inserting the ansatz (16) in the axial vorticity equation (18) and considering the non-penetration condition (13) we obtain an eigenvalue problem for the radial function $\hat{\Psi}$:

$$\omega\left[\frac{d}{ds}\left(\frac{s}{H}\frac{d}{ds}\right)-\frac{m^2}{sH}\right]\hat{\Psi}-2m\frac{s}{H^3}\hat{\Psi}=0. \tag{19}$$

For a given m, the eigensolution is given by the set $(\hat{\Psi}_N^m, \omega_N^m)$ where $N \geq 1$ is an integer number that indicates a particular solution to the radial eigenproblem (19). By considering regularity at the origin $s = 0$ (Lewis and Bellan, 1990), an analytical solution is given by

$$\hat{\Psi}_N^m = s^m H^3 P_{N-1}^{(3/2,m)}(2s^2-1) \tag{20}$$

$$\omega_N^m = -\frac{m}{N(2N+2m+1)+\frac{m}{2}} \tag{21}$$

where $P_n^{(\alpha,\beta)}(x)$ is a Jacobi polynomial (see for example chapter 22 of Abramowitz and Stegun (1965)) and $T_N^m = 2\pi(\omega_N^m)^{-1}$ is the eigenperiod of the N^{th} solution given a certain m. The pre-factor s^m in (20) ensures differentiability of the solution at $s = 0$ for any values of m and the factor H^3 ensures that the azimuthal velocity field remains finite at $s = 1$. Equation (19) is of Sturm-Liouville type (Arfken, Weber, and Harris, 2011) and, complemented by the conditions of regularity at the origin and non-penetration at the equator, it is a self adjoint problem. Therefore the solution (20), (21) is unique and each one of the eigenfunctions (20) corresponds to a distinct eigenvalue (21). Furthermore, as will be illustrated in detail later, it is possible to define a scalar product under which different solutions (20) are orthogonal and therefore form a complete set. These results are in agreement with previous studies (Canet, Finlay, and Fournier, 2014); in particular the eigenperiods are all negative, indicating waves moving eastward, as expected for hydrodynamic Rossby waves contained in a sphere.

IV. AN ALTERNATIVE FORMULATION AND SOLUTION IN OBLATE SPHEROIDS

In Labbé, Jault, and Gillet (2015) an alternative formulation is presented that does not rest on the axial vorticity equation but on the projection of the momentum equation on the

space of the flows with columnar geometry. Here we follow the procedure described in Labbé, Jault, and Gillet (2015) and generalise it to an oblate spheroid of equatorial radius $s = 1$ and vertical axis $b \leq 1$. See figure 1 for the geometry under consideration. The spherical geometry is recovered for $b = 1$. Since we continue working in cylindrical coordinates we need to express the direction of the normal $\mathbf{n}$ to the surface of the spheroid in this coordinate system as now the non-penetration boundary condition is

$$\mathbf{n} \cdot \mathbf{u}|_{\partial V} = 0, \tag{22}$$

where the ∂V is the boundary of the spheroid. The eccentricity of the spheroid is $\epsilon = \sqrt{1 - b^2}$, where the case $\epsilon = 0$ represents a sphere and $\epsilon = 1$ is a spheroid with vanishing height above the equatorial plane. We define the surface of the spheroid by its position z with respect to the equatorial plane

$$z = \pm b\sqrt{1 - s^2} = \pm h, \tag{23}$$

where the positive and negative signs apply on the Northern and Southern hemisphere, respectively, and $h = bH$. This equation is an identity of the form $g(s, z) = 0$ that describes the surface of the spheroid. The normal to the surface can be then be readily calculated as:

$$\mathbf{n} = -\nabla g(s, z) = \mp \mathbf{e}_s b \frac{s}{\sqrt{1 - s^2}} - \mathbf{e}_z. \tag{24}$$

The non-penetration boundary condition (22) in cylindrical coordinates is $u_s n_s + u_z n_z = 0$ which, making use of (24) reduces to

$$u_z = \mp b \frac{s}{\sqrt{1 - s^2}} u_s. \tag{25}$$

We see that the definition (11) satisfies the non-penetration boundary conditions in spheroidal geometries for any value of b. Since the momentum equation in non-dimensional form is still given by (14) following the procedure that leads to the axial vorticity formulation (19) gives the same normal mode equation and the same solution (20)-(21). We now follow Labbé, Jault, and Gillet (2015) and we project the Navier-Stokes equation on the space of the geostrophic flows. This procedure is reminiscent of the one followed in the finite element methods (Durran, 2010) to obtain the weak form of the evolution equations: assuming that the flow $\mathbf{u}(\Psi)$ is defined as in (11) we form the dot product of the Navier-Stokes equation with the test function $\mathbf{u}'(\Psi')$, also expressed as a columnar flow:

$$\mathbf{u}' = \frac{1}{\sqrt{1 - s^2}} \nabla \times (\Psi'(s, \phi)\mathbf{e}_z) - u'_s \frac{sz}{1 - s^2} \mathbf{e}_z \tag{26}$$

and we integrate the resulting equation in the volume V of the spheroid. This leads us to the following:

$$\int_V \mathbf{u}' \cdot \left[\frac{\partial \mathbf{u}}{\partial t} + 2\mathbf{e}_z \times \mathbf{u} + \nabla P \right] dV = 0. \tag{27}$$

By means of integration by parts we now manipulate this equation with the purpose of collecting Ψ' as common factor. We can use the non-penetration boundary condition on ∂V (22), and in particular at the equatorial boundary

$$\Psi(s = 1) = 0, \tag{28}$$

the regularity condition at the origin, requiring that Ψ is proportional to s^m as $s \to 0$, and the incompressibility condition (6). The volume integral over the spheroid can be separated in an integration along the vertical direction, from $-b\sqrt{1-s^2}$ to $b\sqrt{1-s^2}$, and an integration on the equatorial disk, whose surface area is indicated with A. By making use of Gauss' integration theorem the pressure term in (27) vanishes. Manipulating the remaining terms leads to

$$\int_A \Psi' \left[-2\frac{b}{s}\frac{\partial}{\partial s}\left(\frac{s}{H}\frac{\partial}{\partial s}\frac{\partial \Psi}{\partial t}\right) - 2b\left(\frac{1}{s^2 H} + \frac{1}{3}\frac{1}{H^3}b^2\right)\frac{\partial^2}{\partial \phi^2}\frac{\partial \Psi}{\partial t} + 4\frac{b}{H^3}\frac{\partial \Psi}{\partial \phi}\right] dA = 0. \tag{29}$$

where $\int_A dA = \int_0^1 \int_0^{2\pi} s d\phi ds$. Since this integral has to vanish for any value of the test function Ψ' we obtain the following equation:

$$\left[\frac{\partial}{\partial s}\left(\frac{s}{H}\frac{\partial}{\partial s}\right) + \left(\frac{1}{sH} + \frac{s}{3}\frac{1}{H^3}b^2\right)\frac{\partial^2}{\partial \phi^2}\right]\frac{\partial \Psi}{\partial t} - 2\frac{s}{H^3}\frac{\partial \Psi}{\partial \phi} = 0. \tag{30}$$

Compared to the axial vorticity equation this procedure results in an extra term proportional to b^2. This result is consistent with and can be derived from Labbé, Jault, and Gillet (2015) upon substituting H with $h = bH$ in their (equation 13f). Note that this operation leaves the slope $\beta = -(dH/ds)/H$ unchanged. For $b = 0$ the spheroid has no vertical extension and reduces to a 2-D disc. In this case equation (30) reduces to the axial vorticity equation (18) previously obtained, illustrating how the axial vorticity formulation results in an equation that retains no information about the parameter b. Substituting (16) in (30) we obtain an eigenvalue problem with solution:

$$\hat{\Psi}_N^m = s^m H^3 P_{N-1}^{(3/2,m)}(2s^2 - 1) \tag{31}$$

$$\omega_N^m = -\frac{m}{N(2N + 2m + 1) + \frac{m}{2} + \frac{m^2 b^2}{6}}. \tag{32}$$

As expected (32) reduces to (21) for $b = 0$. The geometry of the eigenmodes (20) is however unaffected by the eccentricity of the container. Equation (30) is also a Sturm-Liouville equation. Therefore the considerations illustrated above for equation (19) apply for (30) and the eigenfunctions (31) with eigenvalues (32) form a complete basis set.

It is straightforward to deduce that the solutions $\hat{\Psi}_N^m$ for any given m are orthogonal under the following scalar product:

$$\int_0^1 \hat{\Psi}_N^m(s)\hat{\Psi}_K^m(s)\frac{s}{H^3}ds = \frac{1}{2}\frac{\Gamma\left(N+\frac{3}{2}\right)\Gamma(N+m)}{(N-1)!\left(2N+\frac{1}{2}+m\right)\Gamma\left(N+\frac{3}{2}+m\right)}\delta_{N,K} \equiv ||\hat{\Psi}_N^m||^2\delta_{N,K}. \tag{33}$$

For $b > 0$ corresponding velocities are also orthogonal according to

$$\int_V (\mathbf{u}_N^{m'})^* \cdot \mathbf{u}_K^m dV = -4mbT_N^m||\hat{\Psi}_N^m||^2\delta_{m,m'}\delta_{N,K} \equiv ||\mathbf{u}_N^m||_{b>0}^2\delta_{m,m'}\delta_{N,K}. \tag{34}$$

Here V is the volume of the spheroid defined by a given value of $0 < b \leq 1$, $(\mathbf{u}_K^{m'})^*$ is the complex conjugate of the normal mode $\mathbf{u}_K^{m'} = \hat{\mathbf{u}}_K^{m'}\mathrm{e}^{\mathrm{i}m'\phi}$ and the meridional component of the velocity $\hat{\mathbf{u}}_K^{m'}$ is a complex quantity. For $b = 0$ the spheroid collapses to the equatorial disc and the analogous version of integral (34) would have to be taken over the plane $z = 0$. However in order to make use of (33) and preserve the form of the norm (34) we integrate over the unit sphere. The integrand $(\mathbf{u}_N^{m'})^* \cdot \mathbf{u}_K^m$ is evaluated on $z = 0$ before integration, and the vertical integration is substituted by a multiplication by $2H$. The case $b = 0$ results then in the following orthogonality condition:

$$\begin{aligned}\int_A\int_{-H}^{H}\left[(\mathbf{u}_N^{m'})^* \cdot \mathbf{u}_K^m\right]_{z=0} dzdA &= \int_S 2H\left[(\mathbf{u}_N^{m'})^* \cdot \mathbf{u}_K^m\right]_{z=0} dA \\ &= -4mT_N^m||\hat{\Psi}_N^m||^2\delta_{mm'}\delta_{N,K} \equiv ||\mathbf{u}_N^m||_{b=0}^2\delta_{mm'}\delta_{N,K}.\end{aligned} \tag{35}$$

where T_N^m is now given by (21) and we explicitly indicated the vertical integration from $-H$ to H and the integration over the surface of the equatorial disc A.

V. COMPARISON WITH 3-D CALCULATIONS

A. The spherical case

It is known (Canet, Finlay, and Fournier, 2014; Labbé, Jault, and Gillet, 2015) that for high values of m and low values of N, the QG solution (21) calculated from the axial vorticity equation tends to deviate considerably from the prediction of 3-D calculations. This

is illustrated in figure 2 where the dashed lines are calculated from the formula (21) and the crosses are the corresponding 3-D solution from Zhang *et al.* (2001). The 3-D eigenperiods considered in the figure are the ones closest to the QG solution and those corresponding to equatorially symmetric modes with the lowest vertical complexity. For any given m, this corresponds to the modes with smallest eigenfrequency (in absolute value) which in Zhang and Liao (2004) are referred to as QGIW (Quasi-Geostrophic Inertial Waves) and are the only modes for which a comparison with our columnar oscillations is possible. As shown on the scale of the vertical axis in figure 2, the eigenperiod of the modes considered here can be much longer than the rotation period of the system.

The full lines in figure 2 are the eigenmodes calculated from the formula (32) with $b = 1$. This solution is a better approximation of the 3-D calculations than (21), as also shown in Labbé, Jault, and Gillet (2015). It remains true that the 3-D solution is better approximated by QG modes for high values of N and low values of m. The reason for this is understood by analysing the geometry of the modes (figures 3 and 4). As m increases the maximum is shifted toward the equator, where the QG approximation is expected to deviate the most from the fully 3-D calculations of Zhang *et al.* (2001). In the upper rows of figures 3 and 4 we illustrated this for $N = 1$ and $N = 15$ where the stream function $\hat{\Psi}$ of the QG modes is compared to an equivalent stream function derived from the equatorial projection of the 3-D modes. Guided by (11) we assume that, for a given N and m, there exists a stream function $\Psi^{3D}(s, \phi)$ such that:

$$\frac{1}{2H}\int_{-H}^{H} \hat{u}_s^{3D}(s,z)dz = \frac{\mathrm{i}m}{sH}\hat{\Psi}^{3D}(s) \tag{36}$$

where $u_s^{3D}(s, \phi, z)$ is the cylindrical radial component of the 3-D normal mode calculated according to the formulas of Zhang *et al.* (2001) for the given N and m. The right-hand side of (36) represents a vertical average of the meridional component $\hat{u}_s^{3D}$ and the function $\hat{\Psi}^{3D}(s)$ is represented by the red lines in figures 3 and 4. The agreement with the QG solution is excellent, indicating that the horizontal structure of the inertial modes is reliably reproduced in the QG approach for any N and m. The deviations in the dispersion relation are less pronounced in the higher N modes (like the $N = 15$ mode shown in figure 4) since the high amplitude oscillations are further away from the equator while for low N (see figure 3) the few oscillations are concentrated towards the outer boundary. In the lower rows of figures 3 and 4 we show the meridional structure of the 3-D eigensolution. The

z-independence of the 3-D modes increases with N and decreases with m. For larger N, the boundary conditions can be matched in ever finer regions, allowing the solution over the remaining volume to be almost exactly z-invariant. For large m, the modes are focused close the equator where the QG approximation breaks down. As the 3-D solution shows more vertical dependence, the deviations in the dispersion relation (figure 2) grow larger. That the solution becomes more and more equatorial as m increases was expected from the presence of a pre-factor s^m in both the columnar solution (32) and the 3-D modes of Zhang *et al.* (2001) and due to the condition of regularity that has to be imposed at the origin $s = 0$. Since $s \leq 1$, as m increases the pre-factor is smaller closer to the origin and the modes oscillates preferentially closer to the boundary $s = 1$.

We now briefly highlight the difference between our approach and the 3-D one presented in Zhang *et al.* (2001), who also analysed the slow modes referred to as the QGIW in Zhang and Liao (2004). They note that an approximate frequency of these waves is

$$\omega_G = -\frac{2}{m+2}\left(\sqrt{1+\frac{m(m+2)}{N(2N+2m+1)}}-1\right) \tag{37}$$

which is an explicit rather than the normally implicit formula for the frequency, valid only for the gravest inertial mode given a certain m and N. When one adopts the approximated QGIW frequency (37), a visual comparison such as figure 2 is unchanged. However, we find that in adopting (37) the boundary conditions of the 3-D modes are no longer satisfied, since adherence to the non-penetration boundary condition rests on the use of the exact eigenfrequency, derivable only as roots of a polynomial equation of degree $2N$. On the other hand, the flows (11) always satisfy non-penetration at the boundary and are, of course, independent of the frequency.

When $N \gg m$ the approximate QGIW frequency becomes

$$\omega_G \approx -\frac{m}{N(2N+2m+1)}, \tag{38}$$

the similarities with (21) being striking, showing why the comparison in figure 2 is so good. We should, however, highlight some differences in the form of the eigenfunction, lest a misleading impression be given. In doing so we dispel any notions that the modes we have found are in any way a subset of the true 3-D inertial modes satisfying Poincaré's differential equation. To do so we take as an example the lowest QGIW, namely the $N = 1$ mode, whose

frequency is approximately $-m/(2m+3)$; the form of the fluid motions for this mode are:

$$\begin{aligned} u_s^{3D} &\propto s^{m-1}(1+As^2+Bz^2) \\ u_\phi^{3D} &\propto s^{m-1}(1+Cs^2+Bz^2) \\ u_z^{3D} &\propto s^m z \end{aligned} \tag{39}$$

with known coefficients A, B and C (Zhang *et al.*, 2001). In comparison, our modes have the form:

$$\begin{aligned} u_s &\propto s^{m-1}(1-s^2) \\ u_\phi &\propto s^{m-1}(m(1-s^2)-3s^2) \\ u_z &\propto s^m z \end{aligned} \tag{40}$$

with frequency $-m/(5m/2+3)$ as given by (21). One can see that the vertical flow has the same structure, but the u_s^{3D} and u_ϕ^{3D} components are not z-invariant, as they always are in our formulation. Both formulations adhere to the regularity conditions required for continuity and infinite differentiability at the origin (Lewis and Bellan, 1990).

B. The spheroidal case

In figure 5 we show the same comparison as in figure 2 but for different spheroids defined by different values of b. The QG results are calculated using formula (32) and the 3-D solutions are calculated using the results of Zhang, Liao, and Earnshaw (2004). As in the spherical case, the QG solution is compared with the equatorially symmetric 3-D modes with the lowest vertical complexity. Again we see that with increasing N and for low values of m the agreement between the 3-D and the QG calculation is remarkable. Since the geometrical structures of the modes in the spheroid is the same as in the sphere, the reasons are the same: the QG approximation gives better results when the oscillations are concentrated away from the boundary $s = 1$. We also notice that the agreement in figure 5 is better for very flat spheroids (very low values of b). That is because for very flat spheroids, the vertical structure has a negligible contribution in the dynamics and for the limiting case $b = 0$ the spheroid degenerates into a disk and the geometry of the modes is 2-D, so that both approaches are equally correct. The eigenperiod, on the other hand, is a function of the geometry, as indicated by the presence of the height b in the formula (32). For smaller

values of b the eigenmode with same N and m oscillates with a smaller oscillation period or, equivalently, at a higher frequency.

From figures 2 and 5 we also notice that the dispersion relation is non-monotonic in both the spherical and spheroidal cases. For a given eigenmode N, the eigenperiod curves in the figures reach a minimum at a given m that is a function of the eccentricity of the spheroid. For very oblate spheroids the minimum is reached for very high values of m and is not visible in figure 5.

VI. EFFECT OF VISCOSITY AND BOUNDARY LAYERS

So far we considered only the inviscid form of the momentum equation (5) and the non-penetration boundary condition has been sufficient for the determination of the normal mode solution (31)-(32). For these modes the flow normal to the boundary is zero at the edge of the container and the tangential flows are not constrained. In the presence of viscosity additional boundary conditions must be provided due to the increased order of the momentum equation. These condition can be either no-slip (8) or stress-free (9). In both cases boundary layers with radial extension proportional to $E^{1/2}$ are present (Livermore, Bailey, and Hollerbach, 2016) but their effect on the main flow is reduced in the case of stress-free boundaries. In the no-slip case the velocity field has to vanish across the boundary layer, thus stronger secondary flows are driven that can have a significant effect on the dynamics in the rest of the domain (Greenspan, 1968). In this section we consider both the no-slip (8) and stress-free (9) conditions and calculate corrections to the normal mode eigenperiods (32) and flow structure. We mostly consider the spherical case $b = 1$ but the procedure outlined below can be easily adapted to the generic b case.

A. The no-slip condition

In the present section we investigate the correction required to model viscous effects in the case of no-slip boundary condition. We first follow a well-known asymptotic procedure that is thoroughly illustrated in Kudlick (1966) and Greenspan (1968) that only considers first order viscous terms in the calculation of the eigenfrequencies and decay rates. We then consider a novel approach introduced in Liao and Zhang (2008) in which viscous terms are

treated in a more general fashion and that results in a more precise determination of the decay rates.

1. First order calculations

We follow the classical procedure outlined in chapter 2 of Kudlick (1966) and chapter 2 of Greenspan (1968) and expand the velocity and pressure in the following way:

$$\mathbf{u} = \sum_N C_N \left[(\hat{\mathbf{u}}_N + (2E)^{1/2}\hat{\mathbf{u}}_{N1} + \ldots) + (\hat{\tilde{\mathbf{u}}}_N + (2E)^{1/2}\hat{\tilde{\mathbf{u}}}_{N1} + \ldots) \right] \mathrm{e}^{\mathrm{i}m\phi + s_N t} \tag{41}$$

$$P = \sum_N C_N \left[(\hat{P}_N + (2E)^{1/2}\hat{P}_{N1} + \ldots) + (\hat{\tilde{P}}_N + (2E)^{1/2}\hat{\tilde{P}}_{N1} + \ldots) \right] \mathrm{e}^{\mathrm{i}m\phi + s_N t} \tag{42}$$

where the sum is over the set of normal modes denoted by the index N and the superscript m has been dropped for convenience. The hat variables are functions of the meridional coordinates only, (s, z) or (r, θ) and s_N is:

$$s_N = \mathrm{i}\omega_N + (2E)^{1/2}G + \ldots \tag{43}$$

where we only consider the first order correction term G, which is in general a complex quantity. The leading order terms $\mathbf{u}_N$ and P_N are solution of the normal mode inviscid problem (14) with conditions (6) and (7). Once the viscous terms are being reinstated, we need to consider boundary layer flows $\tilde{\mathbf{u}}_N + (2E)^{1/2}\tilde{\mathbf{u}}_{N1} + \ldots$ and secondary interior flows $(2E)^{1/2}\mathbf{u}_{N1} + \ldots$. The terms indicated by the dots are of order $O(E)$ and are here neglected. The boundary terms are negligible in the interior but are of the same order of magnitude as the interior flow in a thin boundary layer of thickness $O(E^{1/2})$ as they are needed to satisfy the no-slip boundary condition $\mathbf{u} = 0$ at the solid boundary. By mass conservation a secondary interior flow of order $O(E^{1/2})$ is induced. In addition to a flow correction, the eigenfrequencies ω_N need to be corrected for the presence of the Ekman layer. Inserting (41) - (43) into (5) and subtracting the leading order, inviscid solution we obtain evolution equations for $\tilde{\mathbf{u}}_N$ and $\mathbf{u}_{N1}$. The frequency correction G appears in the equation for the secondary interior flow $\mathbf{u}_{N1}$:

$$\mathrm{i}\omega_N \mathbf{u}_{N1} + 2\mathbf{e}_z \times \mathbf{u}_{N1} + \nabla P_{N1} = -G\mathbf{u}_N \tag{44}$$

Following Kudlick (1966), the solution for the interior correction $\mathbf{u}_{N1}$ at the solid boundary is given by:

$$\mathbf{e}_r \cdot \mathbf{u}_{N1}|_{r=1} = \frac{1}{2}\mathbf{e}_r \cdot \nabla \times \left[\mathbf{e}_r \times \mathbf{u}_N \left(\frac{1}{Z_1} + \frac{1}{Z_2} \right) + \mathrm{i}\mathbf{e}_r \times \mathbf{e}_r \times \mathbf{u}_N \left(\frac{1}{Z_1} - \frac{1}{Z_2} \right) \right]_{r=1} . \quad (45)$$

with:

$$Z_1 = -\sqrt{\mathrm{i}(\omega_N - 2(\mathbf{e}_r \cdot \mathbf{e}_z))} \; ; \qquad Z_2 = -\sqrt{\mathrm{i}(\omega_N + 2(\mathbf{e}_r \cdot \mathbf{e}_z))}. \quad (46)$$

In this expression, since only the tangential components of the flow $\mathbf{u}_N$ are of importance, we can substitute $\mathbf{e}_r \times \mathbf{e}_r \times \mathbf{u}_N$ with $-\mathbf{u}_N$ and have a simplified expression. If we set $\omega_N = 0$ in Z_1 and Z_2, the above expression reduces to:

$$\mathbf{e}_r \cdot \mathbf{u}_{N1}|_{r=1} = \frac{1}{2}\mathbf{e}_r \cdot \nabla \times \left[-\mathbf{e}_r \times \mathbf{u}_N - \mathbf{u}_N \frac{\mathbf{e}_z \cdot \mathbf{e}_r}{|\mathbf{e}_z \cdot \mathbf{e}_r|} \right]_{r=1} \frac{1}{|\mathbf{e}_z \cdot \mathbf{e}_r|^{1/2}} \quad (47)$$

which is expression (2.6.13) of Greenspan (1968) derived under the assumption that the time derivatives of the boundary layer flows are negligible. Expression (45) is a generalisation of the Ekman pumping used in QG models (Aubert, Gillet, and Cardin, 2003; Schaeffer and Cardin, 2005; Gillet and Jones, 2006) to implement non-slip boundary conditions. It is important to note that it is impossible to simply impose $\mathbf{u} = 0$ at the CMB when the columnar flow description (11) is implemented, since if the flow is zero at any point on the CMB, it is zero in the whole vertical chord described by the same (s, ϕ).

The correction term G is obtained from the solvability conditions for equation (44). Following appendix A of Kudlick (1966) the result is:

$$G = \frac{\frac{1}{2}(K_1 + K_2)}{\int_V \mathbf{u}_N^* \cdot \mathbf{u}_N dV} \quad (48)$$

where

$$K_1 = \int_{r=1} (\mathrm{i}\omega_N \mathbf{u}_N^* - 2\mathbf{e}_z \times \mathbf{u}_N^*) \cdot \left[\frac{\mathbf{u}_N + \mathrm{i}\mathbf{e}_r \times \mathbf{u}_N}{Z_1} \right] dS \quad (49)$$

$$K_2 = \int_{r=1} (\mathrm{i}\omega_N \mathbf{u}_N^* - 2\mathbf{e}_z \times \mathbf{u}_N^*) \cdot \left[\frac{\mathbf{u}_N - \mathrm{i}\mathbf{e}_r \times \mathbf{u}_N}{Z_2} \right] dS \quad (50)$$

To compute G for the columnar inertial modes we made use of the closed form solution for ω_N and $\mathbf{u}_N$ that can be derived from (31) and (32). The integrals K_1 and K_2 can be

manipulated into the following forms:

$$K_1 = 2\pi \int_{-1}^{1} -(1-x)^{m-1}(1+x)^{m+1}\sqrt{i(\omega_N - 2x)}\left\{x^2(x-1)(2N+2m+3)P_{N-2}^{(5/2,m+1)}(2s^2-1) - [(m+3)x-3]P_{N-1}^{(3/2,m)}(2s^2-1)\right\}^2 dx \tag{51}$$

$$K_2 = 2\pi \int_{-1}^{1} -(1-x)^{m+1}(1+x)^{m-1}\sqrt{i(\omega_N + 2x)}\left\{x^2(x+1)(2N+2m+3)P_{N-2}^{(5/2,m+1)}(2s^2-1) - [(m+3)x+3]P_{N-1}^{(3/2,m)}(2s^2-1)\right\}^2 dx \tag{52}$$

where $x = \cos\theta$. These integrals are then computed for each N and m in arbitrary precision using Mathematica and the denominator of (48) is given in (34). The same computation can be performed for the 3-D inertial modes by making use of the results reported in Zhang *et al.* (2001); an alternative but equivalent expression for the formula (48) are reported in Liao, Zhang, and Earnshaw (2001).

Calculated values of G for the columnar flow solution and for the 3-D modes are compared in figure 6. See also supplementary tables S1 and S2. Note that the real part of G is always negative, indicating that the oscillation is damped by the boundary layers. Since we did not find many calculations for QG inertial modes in the literature, we extended the procedure reported above to the calculation of values of G for 3-D modes of arbitrary vertical structure. In fact equations (48), (49) and (50) are not derived under the assumption of QG flows and are of general validity. A comparison with values reported in the table 1 of Liao and Zhang (2008) shows excellent agreement and confirmed the validity of our method. From figure 6a we observe, as in figure 2, that the QG and 3-D calculations are in excellent agreement for high N and low m but tend to disagree for low values of N and high azimuthal wavenumber m. Interestingly, this conclusion does not appear to hold for the imaginary part of G in figure 6b. Since the imaginary part of G, multiplied by $(2E)^{1/2}$, gives the correction to the inertial modes eigenfrequency, figure 6b suggests that the viscous correction to the eigenfrequency grows with m more steeply for the columnar modes than for the equivalent 3-D solution. The reason for this discrepancy lies in the departure from vertical invariance characteristic of the high m, low N 3-D inviscid modes reported in figure (3). Close inspection of the formulas reported in Zhang *et al.* (2001) reveals that the vertical and equatorial components of the equatorially symmetric, inviscid modes considered here are, at leading order, proportional

to z and z^2 respectively. The s and ϕ components of the same columnar modes described by (11) are independent of z. Given that the QG and 3-D inviscid flows have the same structure when projected on the equatorial plane, the magnitude of the 3-D modes on the boundary $r = 1$ is reduced with respect to the columnar modes. We illustrate this phenomena for the θ component of the inviscid flow for the $N = 1$, $m = 20$ mode, evaluated at $r = 1$, in figure 7a. It seems physically reasonable then, that the viscous effect has a higher influence on the columnar mode than on the 3-D ones. We illustrate this point by introducing the function $f(\theta)$ such that:

$$G = \int_0^{\pi} f(\theta) d\theta. \tag{53}$$

By inspection of (48)- (50) it is clear that:

$$f(\theta) = \pi \sin\theta \left[(\mathrm{i}\omega_N \mathbf{u}_N^* - 2\mathbf{e}_z \times \mathbf{u}_N^*) \cdot \left(\frac{\mathbf{u}_N + \mathrm{i}\mathbf{e}_r \times \mathbf{u}_N}{Z_1} + \frac{\mathbf{u}_N - \mathrm{i}\mathbf{e}_r \times \mathbf{u}_N}{Z_2} \right) \right] \left(\int_V \mathbf{u}_N^* \cdot \mathbf{u}_N dV \right)^{-1} \tag{54}$$

which represents local contribution of the Ekman layer to the frequency correction G. The real and imaginary parts of f are shown in figures (7b) and (7c), respectively, for $N = 1$ and $m = 20$. As expected, the real part of f, whose integral gives the decay rate of the mode, is point-wise negative for both the QG and 3-D cases. On the other hand, the imaginary part has a non-trivial structure and positive and negative contributions cancel each other significantly when integrated over the boundary. This cancellation is less effective for the QG modes explaining why in figure 6b the frequency correction tends to flatten out for the 3-D modes but continues to grow with m for the QG modes. In fact the minima seen to the right and to the left of $\theta = \pi/2$, connected to the minima and maxima of the meridional flow, are deeper with respect to the central maxima in the QG case, reflecting the stronger gradients of the flow on the surface of the sphere.

2. An improved estimate of the decay rate

In Liao and Zhang (2008) a novel approach to the calculation of the viscous contribution to damping and eigenfrequencies has been presented. The procedure does not explicitly rely on the expansions (41), (42) and (43), thus allowing the authors to consider viscous effects from sub-dominant terms and obtain an estimate of the decay rate that is in better agreement with 3-D hydrodynamical numerical simulation. The basic ansatz is that the

velocity field can be expanded as:

$$\mathbf{u} = \sum_N C_N \left[(\hat{\mathbf{u}}_N + \hat{\mathbf{u}}_{N1} + \ldots) + (\hat{\tilde{\mathbf{u}}}_N + \hat{\tilde{\mathbf{u}}}_{N1} + \ldots) \right] \mathrm{e}^{\mathrm{i}m\phi + \mathrm{i}\omega_N t + (d_N + \mathrm{i}\omega_{N1})t} \tag{55}$$

in analogy to expansions (41) - (43), but no explicit assumption is made on the magnitude of the subdominant flows $\mathbf{u}_{N1}$, $\tilde{\mathbf{u}}_{N1}$, decay rate d_N and frequency corrections ω_{N1}. However it is required that $E \ll 1$, $||\mathbf{u}_{N1}|| \ll ||\mathbf{u}_N||$, $||\tilde{\mathbf{u}}_{N1}|| \ll ||\tilde{\mathbf{u}}_N||$, $|d_N| \ll 1$ and $|\omega_{N1}| \ll |\omega_N|$. A similar expansion holds for the pressure as well. The rationale behind this procedure is the break down of the classical expansion (41) - (43) for $|\omega_N| = O(E^{1/2})$, that is, for very low frequency. Given that the QG modes are low frequency inertial modes, the procedure of Liao and Zhang (2008) is of relevance for the present study. Following the steps highlighted in Liao and Zhang (2008) and, crucially, assuming that the viscous stresses at the edge of the boundary layer vanish, ω_{N1} and d_N are found to be:

$$(\mathrm{i}\omega_{N1} + d_N) = \left(\int_V \mathbf{u}_N^* \cdot \mathbf{u}_N dV \right)^{-1} \left[(2E)^{1/2} \frac{1}{2} (K_1 + K_2) - (2E) \int_V \nabla \times \mathbf{u}_N^* \cdot \nabla \times \mathbf{u}_N dV \right], \tag{56}$$

where K_1 and K_2 are defined as in (49) and (50). The first part of this formula is equivalent to (48) and gives the frequency correction and decay rate at order $E^{1/2}$ in the asymptotic expansion. The second part is proportional to an integral that is always real and positive, and contributes to the decay rate at order E. Therefore, formula (56) is equivalent to (48) in estimating the frequency correction, but not for the decay rate.

In figure 8 we show the result of calculation of $-d_N$ for QG and 3-D modes for $E = 10^{-3}$, $E = 10^{-7}$ and $E = 10^{-10}$, as well as the real part of $-(2E)^{1/2}G$ for the QG modes only, for comparison. The agreement between the QG and 3-D calculations is excellent, except for low values of N and high values of m. The differences between the first order approach (48) and the more general (56) is greater at higher E and tends to vanish as E decreases, as the terms proportional to E become subdominant. For $E \simeq 10^{-10}$ there is no visible difference between the two approaches, apart from the higher order modes, indicating that the leading order theory is sufficiently accurate. We also notice that for $E = 10^{-3}$, a value that can be considered moderately low, the assumption $|d_N| \ll 1$ is not satisfied.

B. The stress-free condition

The stress-free case is analysed in a similar way as the no-slip one by considering the first order expansion (Liao, Zhang, and Earnshaw, 2001):

$$\mathbf{u} = \sum_N C_N(\mathbf{u}_N + \mathbf{u}_{N1}) \tag{57}$$

and similarly for the pressure P, where $||\mathbf{u}_{N1}|| = O(E)$. The time dependence can be expressed by the following ansatz:

$$\mathbf{u}(s,\phi,z,t) = \sum_N C_N \left[\hat{\mathbf{u}}_N(s,z) + \hat{\mathbf{u}}_{N1}(s,z)\right] \mathrm{e}^{\mathrm{i}m\phi + (\mathrm{i}\omega_0 + 2E\tau)t}. \tag{58}$$

By inserting (58) in the Navier-Stokes equation (5), neglecting terms smaller than $O(E)$ we obtain:

$$\mathrm{i}\omega_N \mathbf{u}_{N1} + \nabla P_{N1} + 2\mathbf{e}_z \times \mathbf{u}_{N1} = -2E\tau \mathbf{u}_N + 2E\nabla^2(\mathbf{u}_N + \mathbf{u}_{N1}). \tag{59}$$

Following Liao, Zhang, and Earnshaw (2001) we multiply left and right hand sides by $\mathbf{u}_N^*$, integrate over the volume of the sphere. Making use of boundary conditions and of the fact that the normal modes $\mathbf{u}_N$ all satisfy equation (17) with pressure P_N and eigenfrequency ω_N, we obtain:

$$\tau = \frac{\int_V \mathbf{u}_N^* \cdot \nabla^2(\mathbf{u}_N + \mathbf{u}_{N1}) dV}{\int_V \mathbf{u}_N^* \cdot \mathbf{u}_N dV}. \tag{60}$$

The denominator is an integral that can be evaluated exactly, and the numerator is an integral that can be manipulated following Zhang (1994) and making use of the stress-free boundary conditions:

$$\int_V \mathbf{u}_N^* \cdot \nabla^2(\mathbf{u}_N + \mathbf{u}_{N1}) dV = 2\int_{r=1} \mathbf{u}_N^* \cdot \mathbf{u}_N dS - \int_V \nabla \times \mathbf{u}_N^* \cdot \nabla \times \mathbf{u}_N dV. \tag{61}$$

Therefore the calculation of the frequency correction τ does not require the explicit evaluation of the flow $\mathbf{u}_{N1}$. We perform the calculation of the factor τ as done for the no-slip case, making use of both the columnar solution (31)-(32) and the 3-D modes of Zhang *et al.* (2001). The integrals on the right hand side of (61) are calculated with arbitrary precision in Mathematica in both cases for any given N and m. The results are shown in figure 9 and in supplementary tables S3 and S4. As opposed to the no-slip case, the correction is purely real, indicating that there is only a decay factor due to the presence of the boundary layer, but no frequency correction. As for the real part of G (figure 6a), the agreement between

the columnar and the 3-D solutions increases as m is decreased and for high values of N. Interestingly, the value of τ spans many orders of magnitude for different values of m and N. The damping in the case of stress-free boundary condition can therefore be significant for moderate values of E and for modes with significant structure in both s and ϕ. For example, for $N = 10$ the value of τ is of the order 10^4. The damping is of order unity if $E = O(10^{-4})$.

C. The dissipation integral

From the calculations described in the previous sections it is clear that the quantity:

$$\int_V (\mathbf{u}_K^m)^* \cdot \nabla^2 \mathbf{u}_N^m dV \tag{62}$$

is, for $K = N$, often present in the derivation of viscous corrections to the eigenfrequencies of the inviscid problem as, for example, it emerges from the solvability conditions for equations (59). In the general case when both N and K are integers greater than zero and for generic 3-D inertial modes, the quantity (62) is known as the dissipation integral. A known interesting property of the dissipation integral in the spherical case is that it vanishes for $N = K$ (Zhang *et al.*, 2001). In particular it has been shown in Liao and Zhang (2009) that the dissipation integral is zero for $K \geq N$ when considering 3-D inertial modes. This is a property that appears to extend to spheroidal (Zhang, Liao, and Earnshaw, 2004) and ellipsoidal geometries as well (Vantieghem, 2014). In more recent studies it has been demonstrated that the dissipation integral vanishes for $N \leq K+1$ in spheres (Ivers, Jackson, and Winch, 2015) and tri-axial ellipsoids (Ivers, 2017). Although we do not offer a rigorous proof, we calculated, given the formulas (31)-(32) and for a wide range of m and b, that the dissipation integral (62) is zero for $K \geq N$. Thus the result of Zhang *et al.* (2001) and Liao and Zhang (2009) that the $N = K$ terms of the dissipation integral vanishes in the full sphere, also appear to extend to the columnar modes considered here. However, in the 3-D spherical case the non-zero values of the dissipation integral can be both positive and negative. In the case of columnar inertial modes, the integral (58) assumes only positive values for $K < N$.

VII. DISCUSSION AND CONCLUSIONS

We presented an extensive analysis of the inertial modes resulting from the application of the QG approximation to the equations governing the dynamics of a rapidly rotating fluid sphere. In particular we assume that the flows have a prescribed columnar structure (11) that satisfies the conditions of mass conservation and non-penetration at the boundary. For the first time to our knowledge, a completely analytical solution of the eigenmodes and eigenfrequencies solution to the inviscid problem is presented. In order to eliminate the pressure term that appears in the momentum equation (14) we first consider the axial vorticity equation (18), an approach that is commonplace in the development of QG models. Subsequently we investigated an approach introduced in Labbé, Jault, and Gillet (2015) that consists on the projection of the inviscid momentum equation (14) on the space of QG solutions. This technique allowed us to obtain a closed form solution that has a general character and offers interesting insights on the formulation based on axial vorticity equation. The projection (27) results in an additional term arising from the vertical extension of the domain whose effect is to modify the inertial mode eigenfrequencies and bring them closer to the 3-D, QGIW solution. We could demonstrate that the axial vorticity approach corresponds to the case $b = 0$ (a flat disk). Although boundary conditions are encoded into the columnar flow ansatz (11), the fact that the stream function is independent of eccentricity (and the equivalence of the axial vorticity method to projection onto the plane) means that the solution derived from the axial vorticity formalism is completely independent of the eccentricity. This lack of geometric information means that the solutions, for any particular b, are not as accurate as the alternative approach of Labbé, Jault, and Gillet (2015), which involves an integration over the whole spheroid and depends, crucially, on b.

The closed form solution (31)-(32) is in agreement with known numerical results for the spherical case Canet, Finlay, and Fournier (2014); Labbé, Jault, and Gillet (2015) for both $b = 0$ and $b = 1$. Comparison with the relevant 3-D solutions (Zhang *et al.*, 2001) results in well known departures for modes with simple radial structure (low N) and high azimuthal wavenumber m. This departure is explained in terms of the different dependence on the vertical coordinate z of the two solutions.

The calculation of viscous effects in the no-slip case resulted in good agreement with 3-D calculations, with the noticeable exception of the frequency corrections plotted in figure 6b

which illustrates significant differences for all values of N for $m > 10$. On the boundary the QG flows have sharper gradients that results in enhanced viscous effects. Nevertheless, despite the fundamental differences between the two formulations and the uncorrelated ways of deriving the normal mode solutions, we find that the boundary layer calculations and viscous corrections are in remarkable agreement.

Another outstanding feature of the QG solution is the vanishing of the dissipation integral (62) for $K \geq N$, a property that is well known for 3-D solutions but that was not expected under the columnar approximation, due to the aforementioned differences in the two approaches. This might reflect a fundamental property of the Navier-Stokes equation in the spherical domain that is conserved under the QG approximation.

In the future we plan on taking advantage of the analytical nature of (31)-(32) to further study the QG phenomenology of the Earth's outer core. It is for example known (Zhang, 1994, 1995; Zhang and Liao, 2004; Zhang, Liao, and Busse, 2007) that at the onset of convection the geometry and frequency of the convective flows are, at leading order, determined as a superposition of QG inertial modes. We can make use of the results presented on this paper to perform calculations similar to Zhang and Liao (2004) and Zhang, Liao, and Busse (2007) for the onset of thermal convection in presence of either stress-free or no-slip boundaries. The advantage over 3-D calculations lies in the reduced dimensionality of our formulation that offer the possibility to perform calculations at much lower Ekman numbers. Another application of the results presented here will be the development of a QG numerical model for the study of interannual to decadal dynamics in the presence of a magnetic field similarly to the approach of Canet, Fournier, and Jault (2009) and making use of the projection formulation of Labbé, Jault, and Gillet (2015) to handle the momentum equation and improve the resolution of the equatorial dynamics. The fully analytical nature of our solution will prove useful in the formulation of such a numerical model and future studies will be devoted to it.

Acknowledgments

Numerical calculations have been performed on the ETH cluster Euler. We wish to thank Dr Dominique Jault, Dr Nicolas Gillet and their colleagues at Université Grenoble Alpes for fruitful discussions and useful suggestions. We also express our gratitude to Dr

Dominique Jault and an anonymous reviewer whose comments greatly improved the quality of the original manuscript.

Data accessibility

The Mathematica notebook (version 11.0.1.0) used to generate the QGIW solutions in figures 3 and 4 has been uploaded as part of the supplementary material. A pdf document of the same script is also provided as supplementary material.

Funding statement

This study has been supported by the ETH grant number ETH-1412-1 and by the SNF grant number 200020_143596. PWL acknowledges funding from the Natural Environment Research Council (NERC) grants NE/P016758/1 and NE/G0140431.

Author's contributions

This study was originally part of the PhD work of SM, who performed the bulk of the calculations and mathematical derivations under the columnar flow approximation and wrote the first draft of the manuscript. AJ carried out the mathematical derivations and calculations together with SM and helped drafting the manuscript. PWL has provided the first closed form solutions to the inertial mode eigenvalue problem in terms of the Jacobi polynomials and helped drafting the manuscript. All authors gave final approval for publication

Competing interests

The authors have no competing interests.

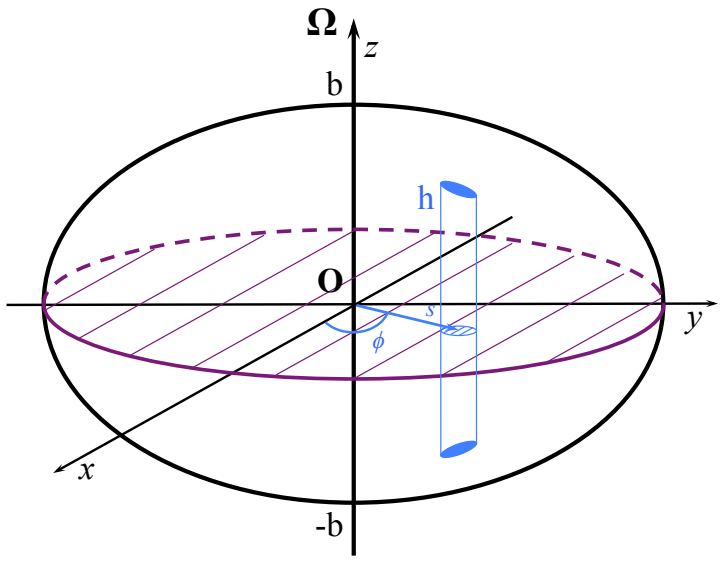

FIG. 1. Spheroidal geometry considered in the calculation of the inertial modes with the formulation proposed in Labbé, Jault, and Gillet (2015). The rotation axis identifies the vertical direction and $\boldsymbol{O}$ is the origin of the coordinate system. We indicate one cylindrical column at a distance s from the rotation axis with its projection on the equatorial plane. The height of the column is $h = b\sqrt{1-s^2} = bH$.

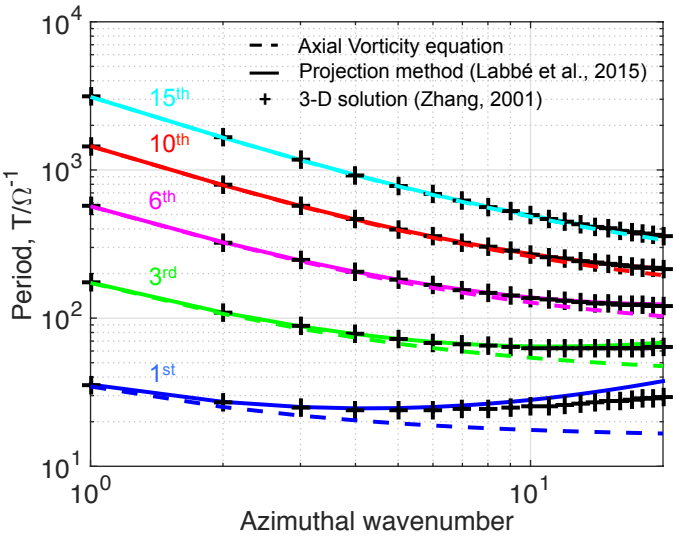

FIG. 2. Dispersion relation for the inertial QG modes in a sphere for different values of the radial solution number N (indicated on the curves) and the azimuthal wavenumber m (on the horizontal axis). Dashed lines are solutions to the axial vorticity equation (19) and given in (21). Full lines are the QG approximations to the inertial modes eigenperiods as calculated via formula (32) with $b = 1$. The black crosses are the corresponding periods for the 3-D modes of Zhang *et al.* (2001) that are best approximated by the QG solutions. On the vertical axis we report the absolute value of the eigenperiods.

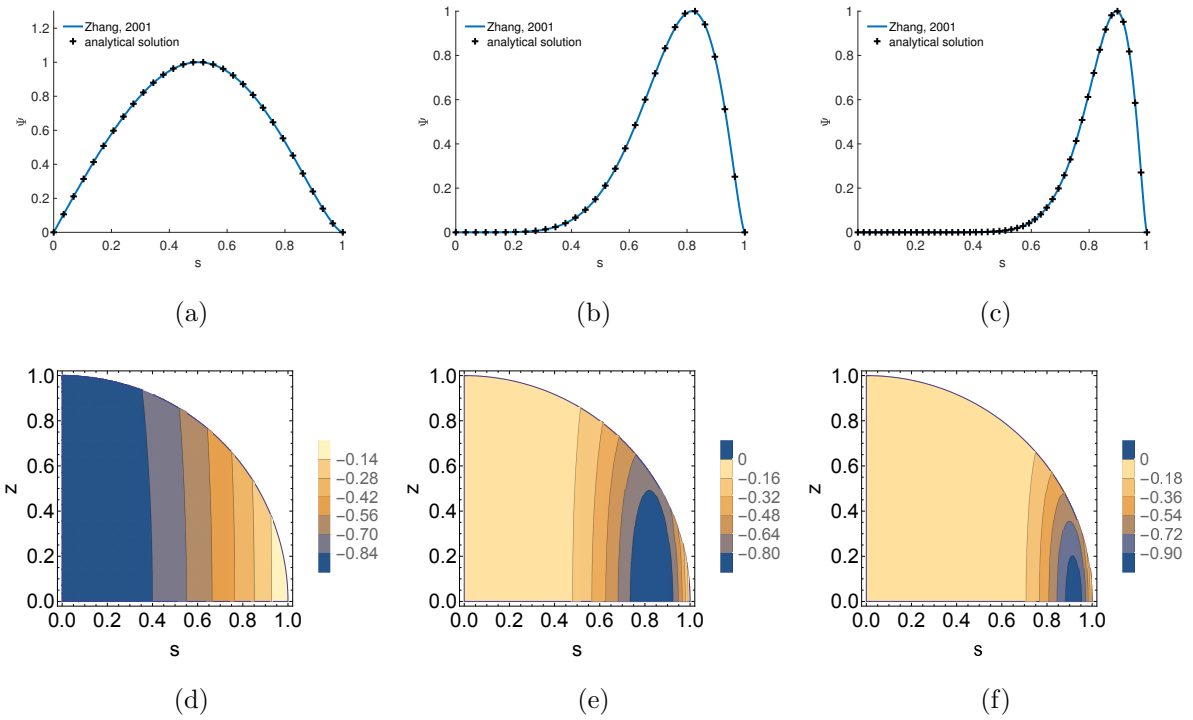

FIG. 3. Geometry of the QG fundamental mode. First row: Comparison of the stream function $\hat{\Psi}$ for the fundamental mode $N = 1$ with $m = 1, 6, 12$ in the left, middle and right plot, respectively. Solid blue lines are the solutions derived from Zhang *et al.* (2001). The black crosses are the theoretical solutions (20). Second row: Corresponding 3-D solutions for the radial velocity obtained from the formulas of Zhang *et al.* (2001).

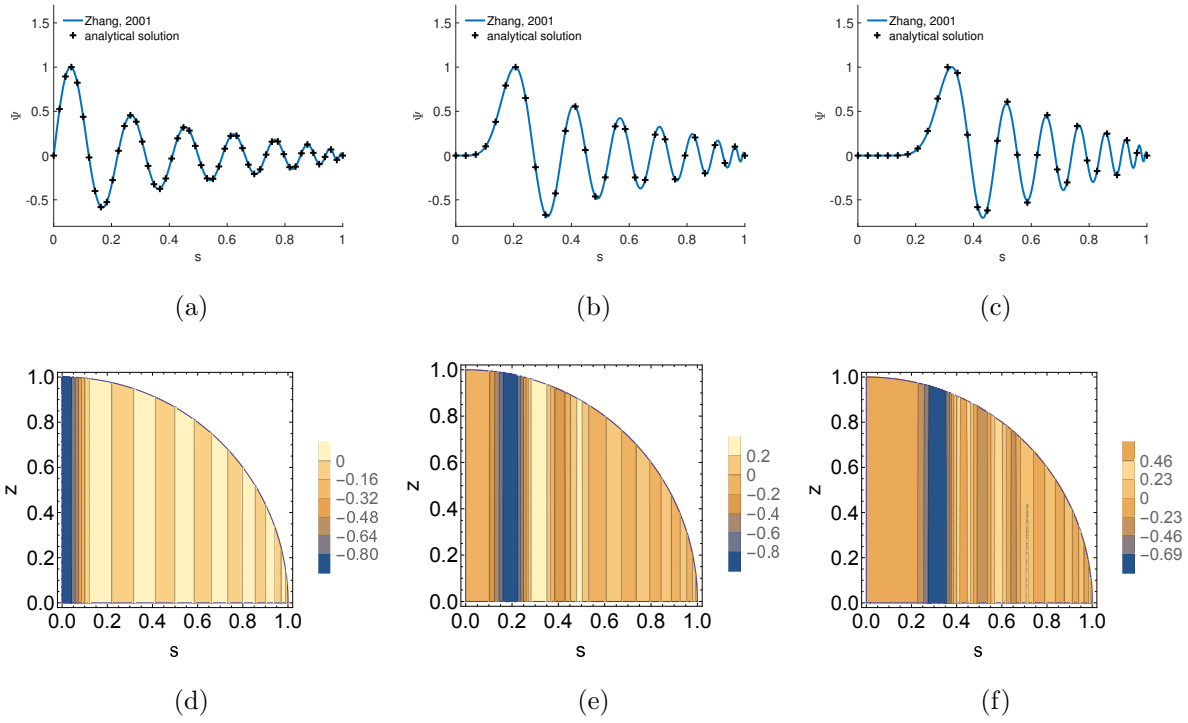

FIG. 4. Geometry of the QG $N = 15$ mode. First row: Comparison of the stream function $\hat{\Psi}$ for the $N = 15$ mode with $m = 1, 6, 12$ in the left, middle and right plot, respectively. Solid blue lines are the solutions derived from Zhang *et al.* (2001). The black crosses are the theoretical solutions (20). Second row: Corresponding 3-D solutions for the radial velocity obtained from the formulas of Zhang *et al.* (2001).

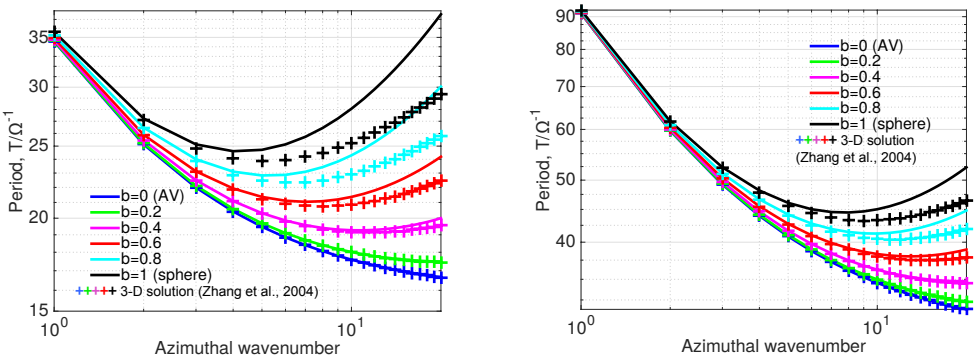

(a) (b)

FIG. 5. Dispersion relation for the inertial QG modes in spheroids of different values of b (indicated by the different line colours) and for $N = 1$ (5a) and $N = 2$ (5b). The full lines are calculated from formula (32) and the crosses are the results from the equatorially symmetric 3-D modes from Zhang, Liao, and Earnshaw (2004) with the lowest vertical complexity and negative eigenfrequency closest to zero. As indicated in the plot, the case $b = 0$ corresponds to the calculation of the normal modes from the axial vorticity equation (AV) and the case $b = 1$ corresponds to the spherical case (see the discussion in the main text).

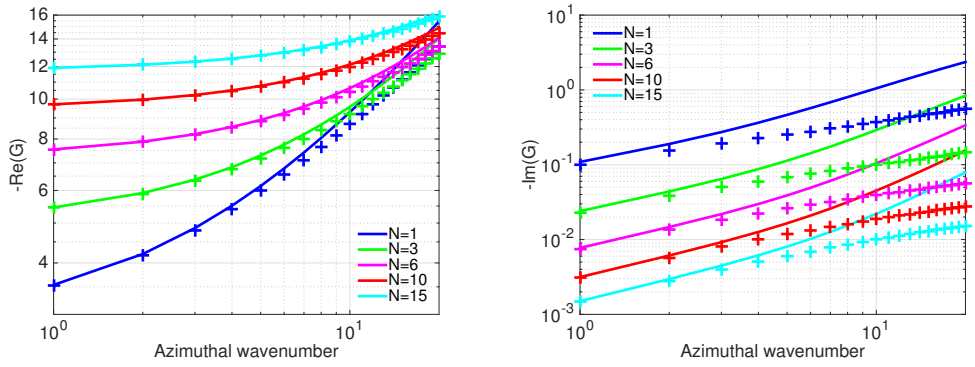

(a) (b)

FIG. 6. Viscous contribution G to the eigenfrequencies solution to the inertial mode problem in the full sphere and for the no-slip case. Results for the columnar modes (full lines), calculated from the formulas (31)-(32) for $b = 1$, and the 3-D modes with the eigenfrequency closest to zero, from Zhang *et al.* (2001) are shown. In (a) the real part of ?G is shown while in (b) the imaginary part of $-G$ is plotted. Note that the real part of G is always negative, indicating that the boundary layer contribution acts to damp the interior solution. The values of G have been calculated according to formula (48) for both the columnar inertial modes and the 3D inertial modes.

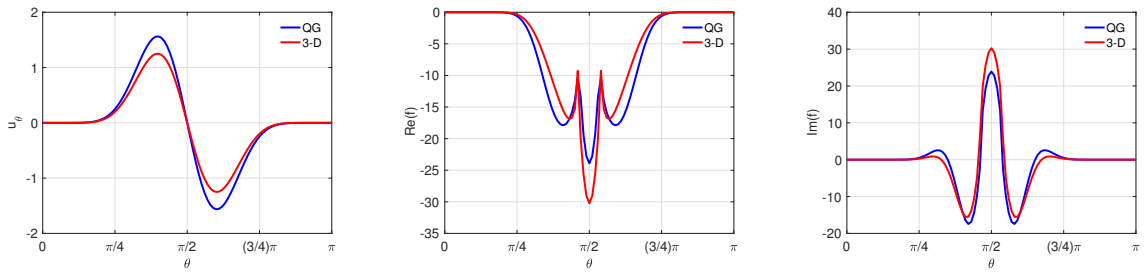

(a) (b) (c)

FIG. 7. (a): Meridional structure of u_θ evaluated at the boundary $r = 1$ for $N = 1$ and $m = 20$ according to both QG (blue line) and 3-D calculations (red line). (b) and (c): respectively, real and imaginary part of the function $f(\theta)$, calculated according to (54), whose integral over the spherical boundary gives the viscous correction G reported in figures 6a and 6b, respectively.

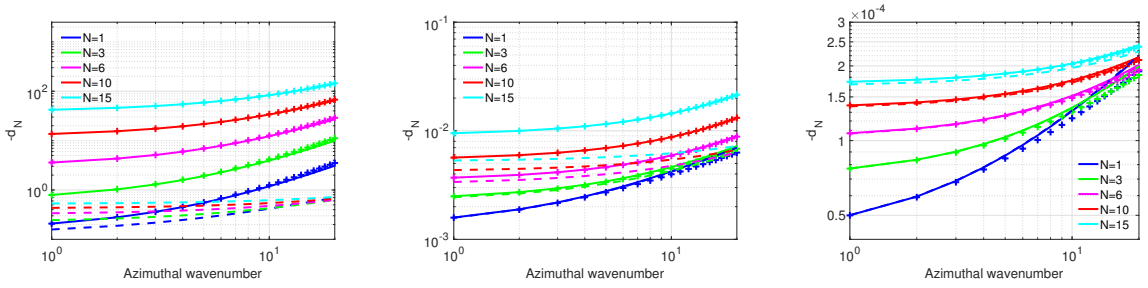

(a) (b) (c)

FIG. 8. Decay rate for $E = 10^{-3}$ (a), $E = 10^{-7}$ (b) and $E = 10^{-10}$ (c) calculated from the real part of the formula (56). The continuous lines and crosses show the result for the QG inertial modes and the equivalent 3-D modes, respectively. The dashed lines show the the real part of (48) for the same modes, for comparison.

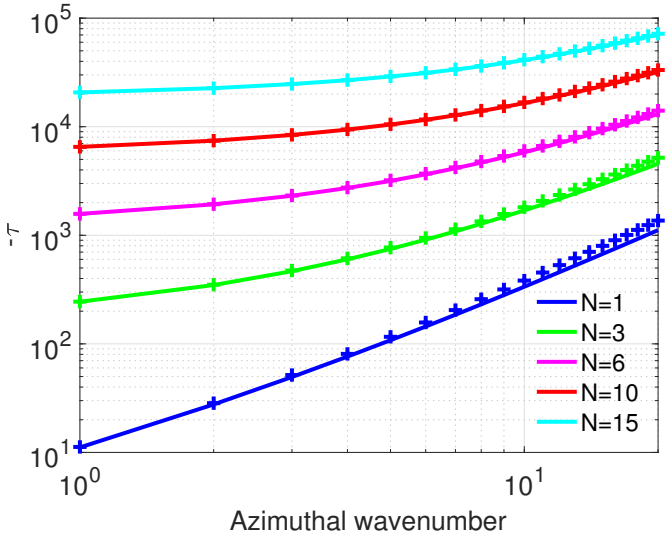

FIG. 9. Decay rate $-\tau$ of the eigenfrequencies solution to the inertial mode problem in a full sphere with stress-free boundaries. Results for the columnar modes (full lines), calculated from the formulas (31)-(32) for $b = 1$, and the 3-D modes with the eigenfrequency closest to zero, from Zhang *et al.* (2001). The values have been calculated according to formula (60) for both the columnar inertial modes and the 3-D inertial modes.

REFERENCES

Abramowitz, M. and Stegun, I. A., *Handbook of Mathematical Functions: with Formulas, Graphs, and Mathematical Tables*, 9th ed. (Dover Publications, New York, NY, 1965).

Arfken, G. B., Weber, H.-J., and Harris, F. E., *Mathematical methods for physicists: a comprehensive guide*, 7th ed. (Academic Press, 2011).

Aubert, J., Gillet, N., and Cardin, P., "Quasigeostrophic models of convection in rotating spherical shells," Geochem. Geophys. Geosyst. **4** (2003), 10.1029/2002GC000456.

Backus, G. and Rieutord, M., "Completeness of inertial modes of an incompressible inviscid fluid in a corotating ellipsoid," Physical Review E **95**, 053116 (2017).

Canet, E., Finlay, C. C., and Fournier, A., "Hydromagnetic quasi-geostrophic modes in rapidly rotating planetary cores," Phys. Earth Planet. In. **229**, 1–15 (2014).

Canet, E., Fournier, A., and Jault, D., "Forward and adjoint quasi-geostrophic models of the geomagnetic secular variation," J. Geophys. Res.: Solid Earth **114**, B11101 (2009).

Cardin, P. and Olson, P., "Chaotic thermal convection in a rapidly rotating spherical shell: consequences for flow in the outer core," Phys. Earth Planet. In. **82**, 235–259 (1994).

Christensen, U. R., "Zonal flow driven by strongly supercritical convection in rotating spherical shells," J. Fluid Mech. **470**, 115–133 (2002).

Davidson, P. A., *Turbulence in Rotating, Stratified and Electrically Conducting Fluids* (Cambridge University Press, 2013).

Durran, D. R., *Numerical Methods for Fluid Dynamics: With Applications to Geophysics* (Springer Science & Business Media, 2010).

Ferraro, V. C., "The non-uniform rotation of the sun and its magnetic field." Mon. Not. R. Astron. Soc. **97**, 458–472 (1937).

Gillet, N., Jault, D., Canet, E., and Fournier, A., "Fast torsional waves and strong magnetic field within the Earth's core," Nature **465**, 74–77 (2010).

Gillet, N. and Jones, C. A., "The quasi-geostrophic model for rapidly rotating spherical convection outside the tangent cylinder," J. Fluid Mech. **554**, 343–369 (2006).

Gillet, N., Schaeffer, N., and Jault, D., "Rationale and geophysical evidence for quasi-geostrophic rapid dynamics within the earth's outer core," Physics of the Earth and Planetary Interiors **187**, 380 – 390 (2011), special Issue: Planetary Magnetism, Dynamo and Dynamics.

Greenspan, H. P., *The Theory of Rotating Fluids* (CUP Archive, 1968).

Guervilly, C. and Cardin, P., "Subcritical convection of liquid metals in a rotating sphere using a quasi-geostrophic model," J. Fluid Mech. **808**, 61–89 (2016).

Hide, R., "Free Hydromagnetic Oscillations of the Earth's Core and the Theory of the Geomagnetic Secular Variation," Philos. Trans. R. Soc. Lond. A **259**, 615–647 (1966).

Hulot, G., Le Mouël, J.-L., and Jault, D., "The flow at the core-mantle boundary," Journal of geomagnetism and geoelectricity **42**, 857–874 (1990).

Ivers, D., "Enumeration, orthogonality and completeness of the incompressible coriolis modes in a tri-axial ellipsoid," Geophysical & Astrophysical Fluid Dynamics , 1–22 (2017).

Ivers, D. J., Jackson, A., and Winch, D., "Enumeration, orthogonality and completeness of the incompressible Coriolis modes in a sphere," J. Fluid Mech. **766**, 468–498 (2015).

Jackson, A., "Intense equatorial flux spots on the surface of the Earth's core," Nature **424**, 760–763 (2003).

Jacobs, J. A., *Geomagnetism*, Vol. 2 (Academic Press, 1987).

Jault, D., "Axial invariance of rapidly varying diffusionless motions in the Earth's core interior," Phys. Earth Planet. In. **166**, 67–76 (2008).

Kageyama, A., Miyagoshi, T., and Sato, T., "Formation of current coils in geodynamo simulations," Nature **454**, 1106–1109 (2008).

King, E. M., Stellmach, S., and Aurnou, J. M., "Heat transfer by rapidly rotating Rayleigh–Bénard convection," J. Fluid Mech. **691**, 568–582 (2012).

Kudlick, M. D., *On transient motions in a contained, rotating fluid*, Ph.D. thesis, MIT, Department of Mathematics (1966).

Labbé, F., Jault, D., and Gillet, N., "On magnetostrophic inertia-less waves in quasi-geostrophic models of planetary cores," Geophys Astro. Fluid. **109**, 587–610 (2015).

Larmor, J., "Possible rotational origin of magnetic fields of Sun and Earth," Elec. Rev **85**, 212 (1919).

Lewis, H. R. and Bellan, P. M., "Physical constraints on the coefficients of Fourier expansions in cylindrical coordinates," J. Math. Phys. **31**, 2592–2596 (1990).

Liao, X. and Zhang, K., "On viscous decay factors for spherical inertial modes in rotating planetary fluid cores: Comparison between asymptotic and numerical analysis," Phys. Earth Planet. In. **169**, 211–219 (2008).

Liao, X. and Zhang, K., "A new integral property of inertial waves in rotating fluid spheres," Proc. Roy. Soc. Lond. A **465**, 1075–1091 (2009).

Liao, X., Zhang, K., and Earnshaw, P., "On the viscous damping of inertial oscillation in planetary fluid interiors," Phys. Earth Planet. In. Dynamics and Magnetic Fields of the Earth's and Planetary Interiors, **128**, 125–136 (2001).

Livermore, P. W., Bailey, L. M., and Hollerbach, R., "A comparison of no-slip, stress-free and inviscid models of rapidly rotating fluid in a spherical shell," Scientific Reports **6**, 22812 (2016).

Malkus, W. V. R., "Hydromagnetic planetary waves," J. Fluid Mech. **28**, 793–802 (1967).

Olson, P., "8.01 - Core Dynamics: An Introduction and Overview," in *Treatise on Geophysics (Second Edition)*, edited by G. Schubert (Elsevier, Oxford, 2015) pp. 1–25, dOI: 10.1016/B978-0-444-53802-4.00137-8.

Pedlosky, J., *Geophysical Fluid Dynamics*, 2nd ed. (Springer-Verlag, New York, 1992).

Roberts, P. H. and Aurnou, J. M., "On the theory of core-mantle coupling," Geophys Astro. Fluid. **106**, 157–230 (2012).

Schaeffer, B. and Cardin, P., "Quasi-geostrophic model of the instabilities of the stewartson layer," Phys. Fluids **17**, 104–111 (2005).

Schaeffer, N. and Cardin, P., "Quasi-geostrophic kinematic dynamos at low magnetic Prandtl number," Earth Planet. Sci. Lett. **245**, 595–604 (2006).

Schmitt, D., "Magneto-inertial waves in a rotating sphere," Geophys Astro. Fluid. **104**, 135–151 (2010).

Vantieghem, S., "Inertial modes in a rotating triaxial ellipsoid," Proc. R. Soc. A **470**, 20140093 (2014).

Yadav, R. K., Gastine, T., Christensen, U. R., Wolk, S. J., and Poppenhaeger, K., "Approaching a realistic force balance in geodynamo simulations," Proceedings of the National Academy of Sciences **113**, 12065–12070 (2016).

Zhang, K., "Spiralling columnar convection in rapidly rotating spherical fluid shells," Journal of Fluid Mechanics **236**, 535–556 (1992).

Zhang, K., "On coupling between the Poincaré equation and the heat equation," J. Fluid Mech. **268**, 211–229 (1994).

Zhang, K., "On coupling between the Poincaré equation and the heat equation: non-slip boundary condition," J. Fluid Mech. **284**, 239–256 (1995).

Zhang, K., Earnshaw, P., Liao, X., and Busse, F. H., "On inertial waves in a rotating fluid sphere," J. Fluid Mech. **437**, 103–119 (2001).

Zhang, K., Lam, K., and Kong, D., "Asymptotic theory for torsional convection in rotating fluid spheres," J. Fluid Mech. **813** (2017), 10.1017/jfm.2017.9.

Zhang, K. and Liao, X., "A new asymptotic method for the analysis of convection in a rapidly rotating sphere," J. Fluid Mech. **518**, 319–346 (2004).

Zhang, K., Liao, X., and Busse, F. H., "Asymptotic solutions of convection in rapidly rotating non-slip spheres," J. Fluid Mech. **578**, 371–380 (2007).

Zhang, K., Liao, X., and Earnshaw, P., "On inertial waves and oscillations in a rapidly rotating spheroid," J. Fluid Mech. **504**, 1–40 (2004).